Refracted Acoustic Communications in Wireless Underwater Sensor Networks with Mobility

S. Blouin[1], M. Barbeau[2] and E. Kranakis[2]

[1]*Underwater Sensing, DRDC Atlantic Research Centre, Nova Scotia, Canada*
[2]*School of Computer Science, Carleton University, Ottawa, Ontario, Canada*

Keywords: Routing, Refraction, Sensor Networks, Mobile Nodes.

Abstract: Routing is a fundamental function of any wireless network. For battery-powered underwater sensors using acoustic waves, routing is even more challenging due to an ever changing and communication-opaque ocean. Herein, we propose a shallow-water routing scheme that adapts to a unique physical phenomena of the medium. In particular, the proposed routing exploits downward and upward refractions for underwater networks comprising mobile nodes. Solutions for node-to-node links are developed before extending the concept to network routing. In particular, necessary and sufficient conditions guaranteeing the existence of a single-hop link through acoustic refraction are derived. Simulations convey results followed by concluding remarks.

1 INTRODUCTION

Routing is a fundamental function of any wireless network because rarely all nodes are within the transmission range of one another. This is especially true for battery-powered underwater network nodes with a barrier-type topology meant to monitor coastlines, track migrating marine mammals, or protect habitats. The main challenge of routing is to identify the chain of nodes used to transfer data from a source to a destination in the most efficient manner.

Underwater acoustic waves propagate further than electromagnetic or optical waves (Heard et al., 2009). Thus, the primary medium for wireless underwater communications is acoustic waves. Unfortunately, underwater acoustic communications are unpredictable due to frequency-dependent attenuation, time-varying multipath effects, large Doppler/delay spreads, and limited bandwidth (Stojanovic and Preisig, 2009). Underwater acoustics are such that significant losses occur due to absorption and spreading (Urick, 1983). In certain underwater environments, the acoustic channel suffers from rapid variations (Blouin and Inglis, 2013). Certain links may be unidirectional. Besides, acoustic paths bend due to varying sound speed in the water column. Those conditions make the selection of the most appropriate underwater route a non-trivial task. Mobility through the underwater medium whose properties change both in time and space exacerbate the problems.

Most underwater routing schemes are derived from terrestrial radio communications. They are rarely optimized for the underwater communication-opaque environment and almost never tailored to the limitations of the medium (Otnes et al., 2012). Among such routing protocols, one finds both proactive (SEAWEB (Rice and Ong, 2010), DSDV (Perkins and Bhagwat, 1994)) and reactive (DSR (Johnson and Maltz, 1996)) schemes. Proactive protocols actively maintain a routing table by periodically exchanging topology information. Reactive protocols search for a topological route only when there exists data to transmit. For battery-powered sensors, reactive protocols are usually preferred from an energy-conservation standpoint, but they do result in additional delays. Many approaches perform *geographic routing*(Karp and Kung, 2000) where data packets are progressively brought closer to the destination at every step. However, with such an approach there is no guarantee of finding a path, thus possibly leading to a *communication void*.

Geographic routing further breaks down in two categories, i.e., *location-aware* or *location-free*, based on the knowledge of the location of the destination node. Most geographic routing protocols in fact require that each node knows its own location, which in turn necessitates a sensor position estimation technique (Li et al., 2010) and its associated hardware and software. Even though multihop transmissions may reduce power consumption (Porto and Stojanovic,

2007), there exists an optimal hop length between routers for a given set of transmission parameters (Zorzi et al., 2008).

We propose a routing scheme exploiting downward and upward refracting phenomena for underwater networks with mobility. The contributions relate to theoretical results defining the existence of refracted paths between two underwater nodes and conditions leading to interference with the ocean surface and bottom. These results constitute the initial steps in addressing a challenging routing problem that minimizes power losses for improving underwater communications.

Section 2 reviews background material. Section 3 presents an approach to exploit refracted paths to establish point-to-point links. Section 4 generalizes the approach to sensor networks with mobile nodes. Simulation results and concluding remarks are provided in Sections 5 and 6. Additional material and proofs are found in appendices.

2 BACKGROUND

2.1 Problem Definition

A generic underwater sensor network configuration, made of both static and mobile nodes, is illustrated in Figure 1. The left-most static node 1 intends to send a message to the right-most mobile node 6. In addition to variable separation distances between sensors, energy losses due to underwater sound propagation should be considered to efficiently solve the routing problem.
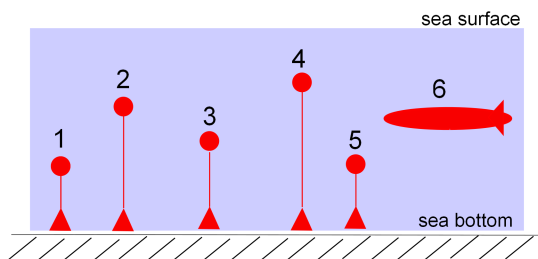

Figure 1: Underwater sensor network.

Shallow-water acoustics are such that routing is extremely challenging due to the multi-path effects, often accompanied by frequency and delay spread (van Walree, 2013). The various acoustic paths linking source 1 to sink 6 can approximately be grouped as occurring through either refraction (curved paths due to the varying speed of sound through the water column) or reflection (acoustic waves bouncing off

the bottom or the surface). Here, we focus on refracted acoustic paths that do not encounter the surface or bottom of the underwater environment. Such paths are called *direct paths*.

Overspread occurs when both frequency and delay spreads disable the demodulation of the received signal (Otnes et al., 2012). Reflected paths tend to lead to larger overspread than refracted paths, especially when multiple reflections occur with a moving sea surface. Moreover, every reflection transfers energy to the boundary it encounters, resulting in additional attenuation. Consequently, usage of refracted paths should be preferred as they may provide savings in terms of power consumption, which is critical for underwater battery-powered wireless sensors.

The prior arguments highlight the importance of exploiting refracted paths as much as possible in the underwater environment. Therefore, the main question of interest is:

How does one exploit refracted paths to route a message from node 1 to node 6 through an underwater sensor network made of both static and mobile nodes?

A unique feature of the aforementioned problem pertains to the fact that the routing strategy needs to adapt to the ever-changing network topology induced by the presence of mobile nodes and also to the varying sound speed profile resulting from a dynamic ocean.

The sound speed profile describes the variation of the speed of sound, $c(z)$, as a function of depth, z. Such profile originates from variations in water temperature, pressure and conductivity (thus salinity) with depth. The sound speed value $c(z)$ usually ranges between $1400\,m/s$ and $1600\,m/s$ (Erbe, 2011), but changes over both time and space. We define the slope of the sound speed profile as

$$g = \frac{d\,c(z)}{dz}, \tag{1}$$

with $c(z)$ in (m/s), z in (m), and g in (1/s or second^{-1}).

2.2 Assumptions

We assume the presence of the following features:

- First-order, i.e., linear, sound speed profiles.
- Flat bottom and surface oceanic boundaries.
- Sensory node with an acoustic transducer having a relatively narrow beamwidth β and a controllable directionality $-\pi/2 < \phi < \pi/2$ with respect to the horizon.
- Nodes equipped with pressure sensors providing a depth measurement.

- Global knowledge of relative distances separating nodes.

Even though not always present in practice, the first-order sound speed profile assumption is a common initial hypothesis in the shallow-water acoustic literature (Katsnelson et al., 2012). Its main impact is that the resulting sound speed profiles reduce to the three categories shown in Figure 2: *isovelocity* (null slope or $g = 0$), *downward refracting* (negative slope or $g < 0$), and *upward refracting* (positive slope or $g > 0$), where c_0 (m/s) denotes the sound speed at the sea surface and g the sound speed profile slope defined in Equation 1. The narrow beamwidth assumption is similar to the focus-beam concept presented in (Nicolaou et al., 2007). Depth measurement capability is assumed in depth-based routing schemes (Hasannezhad et al., 2014). Awareness of relative distances is often assumed in location-aware approaches.
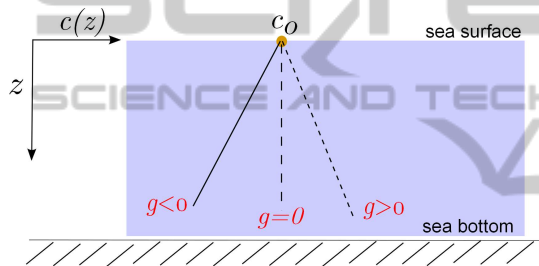

Figure 2: First-order sound speed profiles.

Given the first-order sound speed profile assumption, the sound speed has a slope belonging to one of these categories:

$$\frac{d\,c(z)}{dz} \begin{cases} = 0, & \text{isovelocity,} \\ < 0, & \text{downward refracting, or} \\ > 0, & \text{upward refracting.} \end{cases} \tag{2}$$

Given a sea surface sound speed c_0 (at depth $z = 0$), the linear evolution of sound speed with respect to depth is expressed as

$$c(z) = c_0 + g\,z, \tag{3}$$

with the slope g as defined in Equation 1. We denote node i's depth as z_i and associate a sound speed c_i defined as

$$c_i = c(z_i) = c_0 + g\,z_i, \tag{4}$$

such that $c_i > 0$ for all i's.

3 POINT-TO-POINT LINK

We derive conditions indicating the existence of an acoustic refracted path between any two nodes. In Section 4, this point-to-point link solution is extended by searching all potential paths through the network and selecting the path leading to the lowest transmission loss.

3.1 Straight and Curved Acoustic Rays

We leverage notions from the *Acoustic Ray* theory and thus assumes that appropriate communication frequencies apply (Urick, 1983). An isovelocity sound speed profile leads to straight acoustic rays whereas non-isovelocity cases (upward and downward refracting) generate curved acoustic rays.

We focus on curved acoustic rays. More specifically, the up-coming solution applies to the downward refracting situation, as it is often encountered in shallow waters (Katsnelson et al., 2012).

An important result originating from *Snell's Law* stipulates that in the presence of a linearly varying sound speed profile of constant slope g, any acoustic ray departing from a source node describes an arc of a circle (Urick, 1983). Given an underwater source node i, the center of all circles resulting from different departure angles resides on a *line of centers* whose vertical distance from the source node location is computed as

$$R_i = -\frac{c_i}{g}. \tag{5}$$

According to Equation (5), an isovelocity sound speed profile ($g = 0$) generates arcs of an infinite radius, thus straight rays, whereas downward (respectively, upward) refraction, i.e., $g < 0$ (resp., $g > 0$) locates the line of centers under (resp., above) the sea surface.

3.2 Potential Refracting Scenarios

Figure 3 shows the concepts of the line of centers as well as a generic case with two underwater nodes, i and j. Node i is the source and node j the sink. Note that the water depth is represented by D. The separation distance between nodes i and j is d_{ij}. Such a configuration leads to four potential and mutually-exclusive cases when an acoustic ray departs from node i:

- Case 1: The acoustic ray hits the sea surface before reaching node j.
- Case 2: The acoutic ray overshoots node j.
- Case 3: The acoutic ray directly hits node j.
- Case 4: The acoutic ray undershoots node j, or hits the sea bottom before reaching node j.
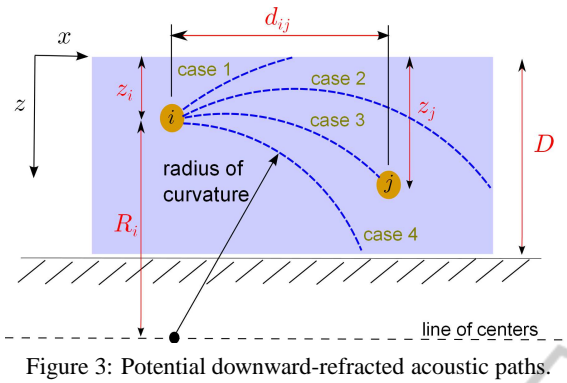
Figure 3: Potential downward-refracted acoustic paths.

3.3 Geometric Solution for Cases 1-to-4

Figure 4 shows (in blue) the two rays acting as the outer envelope for all acoustic rays departing from node i. Given a beamwidth β and a direction ϕ (with respect to the horizon), the envelope determines the angles α_1 and α_2 where

$$\alpha_1 = \phi, \tag{6}$$
$$\alpha_2 = \phi + \beta, \tag{7}$$

such that $-\pi/2 < \alpha_1, \alpha_2 < \pi/2$ which means that acoustic rays are prevented from traveling along the vertical axis and solely interacting with boundaries.
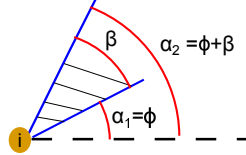
Figure 4: Acoustic rays departing from node i.

The rationale here is that if both value α_1, α_2 fall in the same case, 1, 2, or 4, of Figure 3, then no intermediate directionality angle α_k contained between α_1 and α_2 results in an acoustic ray departing from node i and reaching node j by a refracted path. Similarly, if α_1 coincides with case 4 and α_2 matches case 2, then there exists an intermediate directionality angle $\alpha_1 \leq \alpha_k \leq \alpha_2$ for which an acoustic ray departing from node i reaches node j by a refracted path.

Assuming an acoustic ray departing from node i at an angle α_k where $\alpha_1 \leq \alpha_k \leq \alpha_2$, it is possible to compute the exact location of the corresponding circle center with simple geometry as illustrated in Figure 5. Given that the acoustic ray departing from node i forms a right angle with the line joining node i and its circle center, we can derive R_k, the radius of curvature, and d_k, the horizontal distance separating node i from the center of the circle describing the curved

acoustic ray as follows

$$R_k = \frac{|R_i|}{\cos\alpha_k}, \tag{8}$$
$$d_k = R_i \tan\alpha_k, \tag{9}$$

where R_i originates from Equation (5). Note that the absolute value of R_i in Equation (8) is taken so that the radius of curvature remains positive and to reconcile equations in references (Urick, 1983) and (Lurton, 2010) for downward and upward refracting scenarios.
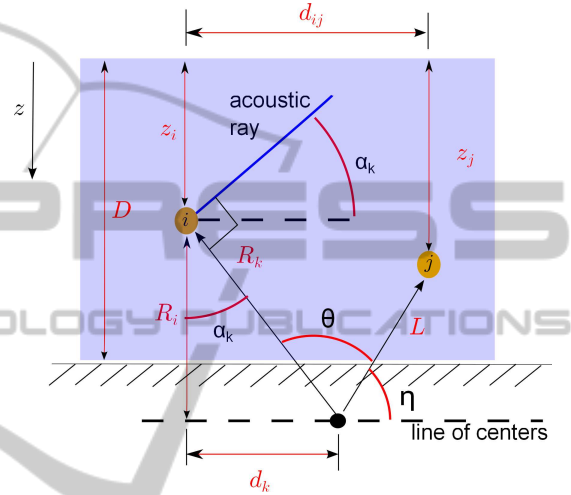

Figure 5: Center of curvature of an acoustic ray.

We next solve the geometry problem and identify conditions leading to Cases 1 through 4.

3.3.1 Case 1

Using node i's location as the center of an (x, z) coordinate system, it can be seen from Figure 5 that if the top of the circle centered at (d_k, R_i) and of radius R_k is above or at sea level then the acoustic ray hits the sea surface, otherwise it does not. Consequently, if $R_i + z_i$, the depth of the circle center, exceeds the length of the curvature radius R_k, i.e.,

$$z_i + R_i > R_k, \tag{10}$$

then the refracted acoustic ray avoids the sea surface. Using the previous argument and the development found in Appendix, we obtain the following result.

Proposition 1

Assume an underwater node i at depth z_i in the presence of a linear sound speed variation as defined in Equation (4). A refracted acoustic ray departing from node i at an angle $|\alpha_i| < \pi/2$ avoids the sea surface if and only if

$$\alpha_i < \alpha_i^{max}, \tag{11}$$

where

$$\alpha_i^{max} = \arccos\left(-sign(g)\left[\frac{c_i}{c_0}\right]\right). \qquad (12)$$

The angle α_i^{max} of Proposition 1 represents the largest departing angle that an acoustic ray can have to avoid the sea surface.

Example 1. The network configuration of Figure 1 is specified through a node depth array $Z = \{z_1, \ldots, z_6\}$ and a node-to-node horizontal separation distance array $d = \{d_{12}, \ldots, d_{16}\}$ with values

$$Z = \{150, 135, 147, 125, 150, 143\} - \lambda,$$
$$d = \{400, 1000, 1600, 1900, 2600 + \delta\},$$

where λ is a depth offset for all sensors, while δ is a range offset for the mobile node only. Environmental conditions are $D = 200$ m, $c_0 = 1500$ m/s, and $g = -0.25$ 1/s. All acoustic transducers have a beamwidth of $\beta = 10^o$ and their directionality angle ϕ takes different values through the following three scenarios.

<u>Scenario 1:</u> With $\lambda = 0$, $\delta = 0$, $\phi = -\beta/2$, Equations (6) and (7) give $\alpha_1 = -\alpha_2 = -5^o$ and α_i^{max} of Equation (12) is (in degrees)

Node i	1	2	3	4	5	6
α_i^{max}	12.8	12.2	12.7	11.7	12.8	12.5

As $\alpha_i^{max} > \max(\alpha_1, \alpha_2) = 5^o$ for all i's, Proposition 1 implies that none of the acoustic rays departing from any node will reach the sea surface.

<u>Scenario 2:</u> By making the environment shallower with $\lambda = 121$, Equation (12) now gives

Node i	1	2	3	4	5	6
$\alpha_i^{max}(degrees)$	5.6	3.9	5.3	2.1	5.6	4.9

so that some acoustic rays departing from nodes 2, 4 and 6 violate the condition of Proposition 1.

<u>Scenario 3:</u> For this scenario, the $\lambda = 121$ value still applies. Slightly changing the directionality angle to $\phi = -\beta/2 - 3^o$ on all nodes alters α_1 and α_2 such that $\alpha_1 = -8^o$ and $\alpha_2 = 2^o$. Given that α_i^{max} values of Equation (12) remain unchanged from the previous scenario, $\max(\alpha_1, \alpha_2) < \alpha_i^{max}$ and no acoustic rays departing from any node hits the sea surface as per Proposition 1.

Example 1 is instructive in that (a) controlling the directionality angle ϕ can help ensure that no acoustic ray disperses its energy by interacting with the sea surface, and (b) there exists a technique for altering ϕ as captured in the next result.

Corollary 2
Assume an underwater node i at depth z_i in the presence of a linear sound speed variation as defined in Equation (4). Given a fixed beamwidth β, Equation (11) of Proposition 1 holds if the directionality angle ϕ satisfies

$$\phi < \alpha_i^{max} - \beta \qquad (13)$$

The proof of Corollary 2 follows from the fact that Equation (13) is equivalent to $\phi + \beta = \alpha_2 < \alpha_i^{max}$ based on Equation (7).

3.3.2 Cases 2, 3, and 4

Assuming that Equation (11) holds, Cases 2, 3, and 4 can be solved using a similar development. Denoting node j's depth as z_j, Figure 5 displays the geometry involved in identifying the distance L separating node j's location from the center of the circle associated with an acoustic ray leaving node i at an angle α_k. Note that Figure 5 represents the particular case where $d_{ij} > d_k$.

Expressing the distance L mathematically gives

$$L = \sqrt{(d_{ij} - d_k)^2 + (z_i + R_i - z_j)^2}. \qquad (14)$$

From Figure 3 and Equation (14), the remaining cases correspond to

$$
\begin{array}{lll}
L < R_k, & \text{ray overshoots node } j \text{ (Case 2)}, & \\
L = R_k, & \text{ray reaches node } j \text{ (Case 3)}, & (15) \\
L > R_k, & \text{ray undershoots node } j \text{ (Case 4)}. &
\end{array}
$$

For Case 3, the following result holds.

Proposition 3
Assume two underwater nodes i, j at depths z_i, z_j in the presence of a linear sound speed variation as defined in Equation (4). A refracted acoustic ray departing from node i at an angle $|\alpha_k| < \pi/2$ and reaching node j exists if and only if

$$L = R_k, \qquad (16)$$

which is equivalent to an acoustic ray departing angle

$$\alpha_k = \arctan\left(\frac{1}{2d_{ij}R_i}\left[d_{ij}^2 + (\Delta z_{ij})^2 + 2\Delta z_{ij}R_i\right]\right). \quad (17)$$

The proof for Proposition 3 can be found in Appendix. Equation (17) is a closed-form solution indicating which angle α_k results in a refracted path between node i and node j. Using the geometry shown in Figure 5, it is possible to compute the arc length S_{ij} of the refracted acoustic path linking node i to node j through

$$S_{ij} = R_k\theta, \qquad (18)$$

117

where R_k is derived as per Equation (8) and the arc angle span θ (rad) shown in Figure 5 is given by

$$\text{if } d_{ij} > d_k \begin{cases} \theta = \alpha_k + 0.5\pi - \eta \\ \eta = \arctan\left(\dfrac{z_i + R_i - z_j}{d_{ij} - d_k}\right), \end{cases}$$

$$\text{if } d_{ij} < d_k \begin{cases} \theta = \alpha_k - 0.5\pi + \eta \\ \eta = \arctan\left(\dfrac{z_i + R_i - z_j}{d_k - d_{ij}}\right), \end{cases} \tag{19}$$

with α_k from Equation (17) and η shown in Figure 5.

4 NETWORK ROUTING

A refracted acoustic route between a source node 1 and a destination node 6 exists if there is a sequence of refracted paths linking node 1 to node 6.

Underwater *transmission loss*, TL, is a measure of the rate at which the sound energy is lost (Urick, 1983) and a common computation is

$$TL = N\log_{10} r - a \cdot r, \tag{20}$$

where N is the coefficient of geometric spreading, r the range or straight-line distance (in meters) from the acoustic source to the destination, and a the absorption coefficient. Given the relatively close proximity between network nodes, it can be assumed that spherical spreading dominates and is captured by injecting $N = 20$ in Equation (20). Frequency-dependent values for a, the absorption coefficient, are shown in Appendix for atmospheric pressure and a temperature of 5° Celsius (Kinsler et al., 1982) (Kinsler et al., 2000). For commercial acoustic modems operating in the 10-30 kHz frequency band (Hasannezhad et al., 2014), the absorption coefficient a varies linearly in the $0.0008 - 0.0076$ db/m range.

We modify Equation (20) to compute transmission loss along a refracted path from node i to j, with arc length given by Equation (18), as follows

$$TL^*_{i\to j} = N\log_{10} S_{ij} - a \cdot S_{ij}. \tag{21}$$

Based on Equation (18) for S_{ij}, Equation (8) for R_k, Equation (5) for R_i, Equation (19) for θ, and Equation (4) for c_i, $TL^*_{i\to j}$ is a nonlinear function $h(\cdot)$ with the following input variables

$$TL^*_{i\to j} = h(a, c_0, d_{ij}, g, N, z_i, z_j, \alpha_k) \tag{22}$$

with α_k from Equation (17) and where all other variables are measured quantities or constants.

5 SIMULATION RESULTS

We apply the previous results of Section 3 to the underwater network configuration of Figure 1.

Example 2. Similar to Example 1, environmental conditions are $D = 200$ (m), $c_0 = 1500$ (m/s), and $g = -0.25$ (1/s). In Equation (21), $N = 10$ given the shallow water context and $a = 0.0043$ as acoustic communications are assumed to occur around 25 kHz. The network configuration is specified by a node depth array $Z = \{z_1, \ldots, z_6\}$ and a separation distance array $d = \{d_{12}, \ldots, d_{16}\}$ defined as

$$Z = \{150, 135, 147, 125, 150, 143\} - \lambda,$$
$$d = \{400, 1000, 1600, 1900, 2600 + \delta\},$$

where $\lambda = 0$ and $\delta = 0$. From the distance array given above, any node-to-node distance d_{ij} can be derived as shown in Appendix. All sensors have a beamwidth of $\beta = 10^o$ and directionality angle $\phi = -0.5\beta$. Table 1 lists all sixteen different configurations of forward routes departing from node 1 and reaching node 6.

Table 1: Possible forward routes between node 1 and 6.

#	Route
1	$1 \to 6$
2	$1 \to 2 \to 6$
3	$1 \to 3 \to 6$
4	$1 \to 4 \to 6$
5	$1 \to 5 \to 6$
6	$1 \to 2 \to 3 \to 6$
7	$1 \to 2 \to 4 \to 6$
8	$1 \to 2 \to 5 \to 6$
9	$1 \to 3 \to 4 \to 6$
10	$1 \to 3 \to 5 \to 6$
11	$1 \to 4 \to 5 \to 6$
12	$1 \to 2 \to 3 \to 4 \to 6$
13	$\mathbf{1 \to 2 \to 3 \to 5 \to 6}$
14	$1 \to 2 \to 4 \to 5 \to 6$
15	$1 \to 3 \to 4 \to 5 \to 6$
16	$1 \to 2 \to 3 \to 4 \to 5 \to 6$

Figure 6 shows the α_k values of Proposition 3 insuring a direct refracted path between two nodes whose numbers are given on the horizontal axis.
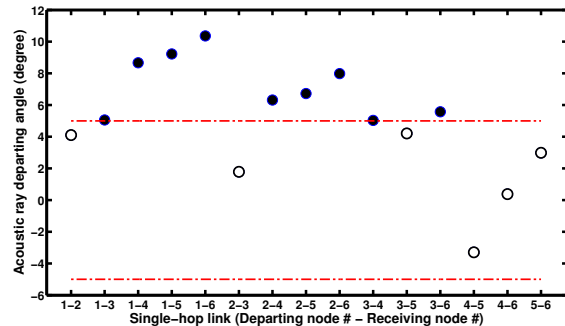

Figure 6: Angles ensuring a refracted path between nodes.

Given that acoustic rays are restricted to depart at angles between $+5^o$ and -5° (indicated by red dashed lines in Figure 6), only links $1 \to 2$, $2 \to 3$, $3 \to 5$, $4 \to 5$, $4 \to 6$, and $5 \to 6$ satisfy this constraint and are indicated by hollow circular markers. Consequently, only route # 13 of Table 1 is actually feasible given the present constraints.

Figure 7 shows the summation of individual transmission loss along the routes of Table 1 using Equation (21) for each individual single-hop link. Route # 13, the only feasible one, has an overall transmission loss of 204 dB, which is significant.
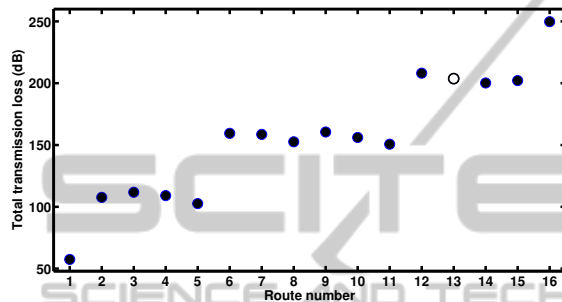

Figure 7: Overall transmission loss over all routes.

From Figure 6, it can be seen that augmenting the beamwidth β from 10° to 12° would incorporate links $1 \to 3$, $3 \to 4$ and $3 \to 6$ which in turn, enables route # 3, i.e., $1 \to 3 \to 6$, whose overall transmission loss is 112 dB, a gain of 92 dB due to a 2° increase in beamwidth.

6 CONCLUSION

This publication proposes a routing scheme exploiting downward and upward refracting phenomena for underwater networks with mobile nodes.

The proposed technique presents an approach using refracted paths to establish node-to-node links and extends those results to a routing problem in a sensor network with mobile nodes. Both theoretical and practical results are derived. In particular, necessary and sufficient conditions guaranteeing the existence of a single-hop link through an acoustic refracted path are derived.

Examples and simulations illustrate how important are the network configuration and the available steering capability of the acoustic energy.

REFERENCES

Blouin, S. and Inglis, G. (2013). Toward distributed noise-source localization for underwater sensor network. In *Proceedings of the IET Intelligent Signal Processing (ISP) conference*, pages 1–6, London, UK.

Erbe, C. (2011). *Underwater Acoustics: Noise and the Effects on Marine Mammals, A Pocket Handbook*. Jasco Applied Science, 3rd edition. —www.jasco.com—.

Hasannezhad, B., Barbeau, M., Blouin., S., Cervera, G., Garcia-Alfaro, J., and Kranakis, E. (2014). Simulation of underwater communications with colored noise approximation and mobility. submitted to the 28th annual IEEE Canadian Conference on Electrical and Computer Engineering (CCECE2015).

Heard, G., Desharnais, F., Ebbeson, G., Fleming, R., and Schattschneider, G. (2009). The use of underwater communication networks in fixed and mobile sensing systems. In *Underwater Acoustic Measurements*, pages 597–604, Nafpilon, Greece.

Johnson, D. and Maltz, A. (1996). *Mobile Computing*. Kluwer Academics Publishers.

Karp, B. and Kung, H. (2000). GPSR: greedy perimeter stateless routing for wireless networks. In *Proceedings of the 6th annual international conference on Mobile computing and networking (MobiCom)*, pages 243–254.

Katsnelson, B., Petnikov, V., and Lynch, J. (2012). *Fundamentals of Shallow-water Acoustics*. Springer.

Kinsler, L., Frey, A., Coppens, A., and Sanders, J. (1982). *Fundamentals of Acoustics*. John Wiley & Sons, Inc., third edition. pages 158-160 (model from Fisher and Simmons, J. Acoust. Soc. Am., 62, 558, 1977).

Kinsler, L., Frey, A., Coppens, A., and Sanders, J. (2000). *Fundamentals of Acoustics*. John Wiley & Sons, Inc., fourth edition. pages 226-228.

Li, Z., Li, R., Wei, Y., and Pei, T. (2010). A survey of localization techniques in wireless sensor networks. *Information Technology Journal*, 9(8):1754–1757.

Lurton, X. (2010). *An Introduction to Underwater Acoustics*. Springer-Verlag, Berlin, 2nd edition.

Nicolaou, N., See, A., Cui, J., and Maggiorini, D. (2007). Improving the robustness of location-based routing for underwater sensor networks. In *Proceedings of the MTS/IEEE Oceans*, pages 1–6, Vancouver (B.C.), Canada.

Otnes, R., Asterjadhi, A., Casari, P., Goetz, M., Husoy, T., Nissen, I., Rimstad, K., van Walree, P., and Zorzi, M. (2012). *Underwater Acoustic Networking Techniques*. Springer.

Perkins, C. and Bhagwat, P. (1994). Highly dynamic destination-sequenced distance-vector routing (DSDV) for mobile computers. *ACM SIGCOMM Comput. Cummun. Rev.*, 24(4):234–244.

Porto, A. and Stojanovic, M. (2007). Optimizing the transmission range in an underwater acoustic network. In *Proceedings of the MTS/IEEE Oceans*. Vancouver (B.C.), Canada.

Rice, J. and Ong, C. (2010). A discovery process for initializing underwater acoustic networks. In *Proceedings of the Fourth International conference on Sensor Technologies and Applications*, pages 408–415.

Stojanovic, M. and Preisig, J. (2009). Underwater acoustic communication channels: Propagation models and

statistical characterization. *IEEE Communication Magazine*, 47:84–89.

Urick, R. J. (1983). *Principles of Underwater Sound*. Mc-Graw Hill, 3rd edition.

van Walree, P. (2013). Propagation effects in underwater acoustic communication channel. *IEEE Journal of Oceanic Engineering*, 38(4):614–631.

Zorzi, M., Casari, P., Baldo, N., and Harris, A. (2008). Energy-efficient routing schemes for underwater acoustic networks. *IEEE J. Selected Areas in Comm.*, 26(9):1754–1766.

APPENDIX

Proof of Proposition 1

$z_i + R_i > R_k \Rightarrow \alpha_i < \alpha_i^{max}$: Using Equations (4) and (5), the left-hand side of Equation (10) becomes

$$z_i + R_i = z_i - \frac{c_i}{g} = z_i - \frac{c_0 + g z_i}{g} = -\frac{c_0}{g}.$$

Given that $c_i > 0$ for all i's, that $-\pi/2 < \alpha = \alpha_k < \pi/2$ or $\cos\alpha > 0$, and Equation (8), the right-hand side of Equation (10) expands as

$$
\begin{aligned}
R_k &= \frac{|R_i|}{\cos\alpha} = \frac{c_i}{|g|} \cdot \frac{1}{\cos\alpha} = \frac{c_0 + g z_i}{|g|} \cdot \frac{1}{\cos\alpha} \\
R_k &= \left(\frac{c_0}{|g|} + z_i \, \text{sign}(g) \right) \frac{1}{\cos\alpha} \\
&= \frac{c_0}{|g|\cos\alpha} + \frac{z_i \, \text{sign}(g)}{\cos\alpha}
\end{aligned}
$$

so that Equation (10) can be re-written as

$$-\frac{c_0}{g} > \frac{c_0}{|g|\cos\alpha} + \frac{z_i \, \text{sign}(g)}{\cos\alpha}$$

which after manipulations becomes

$$-\frac{c_0}{g} - \frac{c_0}{|g|\cos\alpha} > \frac{z_i \, \text{sign}(g)}{\cos\alpha},$$

$$-\frac{c_0}{g} \left[1 + \frac{1}{\text{sign}(g)\cos\alpha} \right] > \frac{z_i \, \text{sign}(g)}{\cos\alpha},$$

$$-\frac{c_0}{g \, \text{sign}(g)} [\text{sign}(g)\cos\alpha + 1] > z_i \, \text{sign}(g),$$

$$\text{sign}(g)\cos\alpha + 1 < \frac{g z_i \, \text{sign}^2(g)}{-c_0} = \frac{g z_i}{-c_0},$$

$$\cos\alpha < \frac{1}{\text{sign}(g)} \left[\frac{g z_i}{-c_0} - 1 \right] = -\frac{1}{\text{sign}(g)} \left[\frac{c_i}{c_0} \right].$$

$z_i + R_i > R_k \Leftarrow \alpha_i < \alpha_i^{max}$: Through contradiction, we show that $z_i + R_i \leq R_k \Rightarrow \alpha_i \geq \alpha_i^{max}$. Using the previous development, it follows that

$$-\frac{c_0}{g} \leq \frac{c_0}{|g|\cos\alpha} + \frac{z_i \, \text{sign}(g)}{\cos\alpha}$$

which through manipulations becomes

$$\cos\alpha \geq -\frac{1}{\text{sign}(g)} \left[\frac{c_i}{c_0} \right].$$

thus

$$\alpha \geq \arccos\left(-\frac{1}{\text{sign}(g)} \left[\frac{c_i}{c_0} \right] \right) = \alpha_i^{max}.$$

Proof of Proposition 3

($\Rightarrow$) Assume that nodes i, j are linked through an acoustic ray departing at angle $|\alpha_k| < 0.5\pi$ from node i. From Equation (8), the radius of curvature of the acoustic ray departing from node i is R_k. From Snell's Law and the constant slope g, the acoustic ray describes an arc of a circle meaning that the radius of curvature for the entire arc remains equal to R_k, thus $L = R_k$.

($\Leftarrow$) If $L = R_k$, then both nodes i, j are located on the perimeter of a circle of radius R_k. Consequently, both nodes are linked by an acoustic ray given Snell's Law and the constant slope g. The departing angle α_k follows from the relationship between R_k and α_k through Equation (8) and the fact that $|\alpha_k| < 0.5\pi$.

Replacing L by R_k in Equation (14) and putting it to the square gives

$$(R_k)^2 = (d_{ij} - d_k)^2 + (z_i + R_i - z_j)^2,$$

which after replacing R_K and d_k by their respective expression in (8) and (9) leads to

$$\left(\frac{R_i}{\cos\alpha_k} \right)^2 = (d_{ij} - R_i \tan\alpha_k)^2 + (z_i + R_i - z_j)^2.$$

Re-labeling $z_i - z_j$ in the previous Equation by Δz_{ij} and expanding the right-hand side results in

$$
\begin{aligned}
\left(\frac{R_i}{\cos\alpha_k} \right)^2 &= (d_{ij} - R_i \tan\alpha_k)^2 + (\Delta z_{ij} + R_i)^2 \\
\frac{R_i^2}{\cos^2\alpha_k} &= d_{ij}^2 - 2 d_{ij} R_i \tan\alpha_k + R_i^2 \tan^2\alpha_k + \ldots \\
&\quad (\Delta z_{ij})^2 + 2\Delta z_{ij} R_i + R_i^2
\end{aligned}
$$

Grouping all R_i^2 terms on the left-hand side gives

$$R_i^2 \left[\frac{1}{\cos^2\alpha_k} - 1 - \tan^2\alpha_k \right] = d_{ij}^2 - 2 d_{ij} R_i \tan\alpha_k + \ldots$$
$$(\Delta z_{ij})^2 + 2\Delta z_{ij} R_i$$

so that the new left-hand term equals zero thus leaving the following expression

$$0 = d_{ij}^2 - 2 d_{ij} R_i \tan\alpha_k + (\Delta z_{ij})^2 + 2\Delta z_{ij} R_i$$

which if re-arranged so as to extract α_k leads to Equation (17).

Node-to-node Distances

Node-to-node distances can be derived as follows

$$d_{23} = d_{13} - d_{12}, \quad d_{35} = d_{15} - d_{13},$$
$$d_{24} = d_{14} - d_{12}, \quad d_{36} = d_{16} - d_{13},$$
$$d_{25} = d_{15} - d_{12}, \quad d_{45} = d_{15} - d_{14},$$
$$d_{26} = d_{16} - d_{12}, \quad d_{46} = d_{16} - d_{14},$$
$$d_{34} = d_{14} - d_{13}, \quad d_{56} = d_{16} - d_{15}.$$

Absorption Coefficient

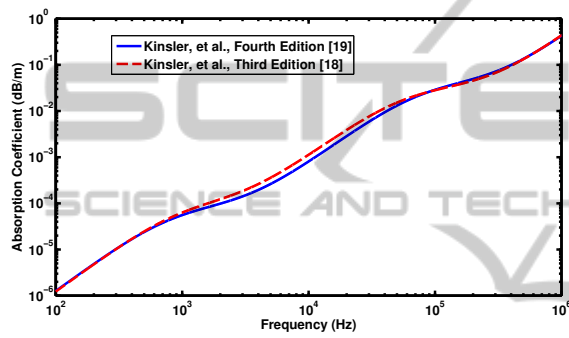Figure 8 displays the absorption coefficient for one atmosphere and a temperature of 5 degrees Celsius.

Figure 8: Absorption coefficient (1 atm., 5°C).